American Journal of Energy Engineering
2022; 10(3): 53-67
http://www.sciencepublishinggroup.com/j/ajee
doi: 10.11648/j.ajee.20221003.11
ISSN: 2329-1648 (Print); ISSN: 2329-163X (Online)

Optimizing Structures Based on Chalcopyrite Materials for Photovoltaic Applications

El Hadji Mamadou Keita*, Fallou Mbaye, Bachirou Ndiaye, Chamsdine Sow, Cheikh Sene, Babacar Mbow

Physics Department, Faculty of Science and Technology, University Cheikh Anta Diop, Dakar, Senegal

Email address:

elouazy@hotmail.fr (El H. M. Keita)

*Corresponding author

To cite this article:

El Hadji Mamadou Keita, Fallou Mbaye, Bachirou Ndiaye, Chamsdine Sow, Cheikh Sene, Babacar Mbow. Optimizing Structures Based on Chalcopyrite Materials for Photovoltaic Applications. *American Journal of Energy Engineering*. Vol. 10, No. 3, 2022, pp. 53-67.
doi: 10.11648/j.ajee.20221003.11

Received: May 26, 2022; **Accepted**: June 27, 2022; **Published**: July 12, 2022

Abstract: In this work we study the importance of optimizing the parameters of photoconductive layers to improve the efficiency of a photovoltaic cell. We compare the evolution of the performance of solar cells based on chalcopyrite materials by considering a non-decreasing band gap structure named model (a) based on the structure $ZnO(n^+)/CdS(n)/CuInSe_2(p)/CuInS_2(p^+)$ and a decreasing band gap structure named model (b) based on the structure $ZnO(n^+)/CdS(n)/CuInS_2(p)/CuInSe_2(p^+)$. The two structures are composed of 4 layers named respectively region 1, region 2, region 3 (base), region 4 (substrate); between regions 2 and 3 is located the space charge region (SCR) where exists a high electric field. The calculation of the external quantum efficiency of the cell and the short-circuit photocurrent density by numerical calculation are established by using the continuity equation of charge carriers and parameters such as the absorption coefficient, diffusion length which models the purity of the material, recombination velocities at the surface and at the interface which models their states, the thicknesses of the different layers, the solar irradiation. The results obtained applied to models (a) and (b), are presented in the form of tables and curves widely analyzed and commented. Considering first the same standard parameters, the model (a) whose absorption threshold is localized in the space charge region and the base, gives the best performance compared to model (b) whose absorption threshold is localized in the substrate. However, the optimization of the parameters, shows an improvement of the performances of the two models but above all a great evolution of the performances of the model (b) which external quantum efficiency becomes appreciably equal to that of the model (a). The short-circuit photocurrent density for solar spectra (AM0, AM1, AM1.5) evolves from (44.92 $mA.cm^{-2}$; 33.031 $mA.cm^{-2}$; 30.179 $mA.cm^{-2}$) → (48.119 $mA.cm^{-2}$; 35.155 $mA.cm^{-2}$; 32.188 $mA.cm^{-2}$) for the model (a), and evolves from (24.525 $mA.cm^{-2}$; 19.309 $mA.cm^{-2}$; 17.507 $mA.cm^{-2}$) → (46.841 $mA.cm^{-2}$; 34.303 $mA.cm^{-2}$; 31.388 $mA.cm^{-2}$) for the model (b).

Keywords: Solar Cell, Chalcopyrite Materials, Structure Parameter Optimization, Efficiency

1. Introduction

Solar energy exploited by photovoltaic cells is radiated over a wide range of wavelengths (covering the whole of the visible plus a part of UV and IR range). This radiation is generally represented by an irradiance spectrum versus the wavelength. The performance of a photovoltaic cell depends on its geographical position. To avoid confusion, a standardization has been introduced by defining reference solar spectra. The notion of Air-mass (AM) was therefore established in order to be able to compare the different spectra used. The solar spectrum in space corresponds to the air-mass value 0 (AM0), while the value 1 (AM1) corresponds to the solar spectrum received on Earth when the Sun is at the zenith. When the sun makes an angle of 48.2 ° with respect to the zenith, the spectrum received on Earth is called AM1.5. The photon fluxes Φ (λ) which correspond to these reference irradiance spectra are shown in figure 7. The integration of irradiance over the entire spectrum allows to obtain the power density (in $W.m^{-2}$) supplied by the radiation. The integration over the entire spectrum of the product of the

photon flux by the external quantum efficiency allows to obtain the short-circuit photocurrent density. The calculation is done by using the continuity equation of charge carriers and parameters such as the absorption coefficient, diffusion length, diffusion coefficient, recombination velocities at the surface and at the interface, the thicknesses of the different layers, the solar irradiation.

The ternary compounds $CuInSe_2$ and $CuInS_2$ belong to the semiconductor family I-III-VI_2 and are increasingly promising for the mass production of photovoltaic modules with a low manufacturing cost and a various techniques of growth and stable devices, they have semiconductor properties under the chalcopyrite structure [1-9]. The chalcopyrite structure corresponds to a regular arrangement of Cu^+ and In^{3+} cations in their sub-lattice. These two materials have quite similar crystalline parameters, band gaps suitable for solar cell operations (in the order of 1.04 eV for $CuInSe_2$ and 1.5 eV for $CuInS_2$) [10-13]. They have also high optical absorption coefficients over the entire solar spectrum covering the visible range which allows a low absorber layer thickness varying from 1 to 3 µm [14-15]. The Se / S substitution also allows to produce quaternary alloys which can pass the band gap between 1.04 eV and 1.57 eV) and an adjustment of the lattice parameters [16-20].

Solar cells based on $CuInS_2$/$CuInse_2$ are generally in the heterojunction type, that is to say the p and n regions are formed by different materials. The $CuInS_2$/$CuInse_2$ layers are doped p-type generally with an excess of sulfur/selenium, a deficit leads to the n-type [21-22]. The doping rate can vary between 10^{16} and 10^{17} cm^{-3} and diffusion length of electrons in the order of micron. The composition of the cell is generally as follows: Mo (or ITO) / $CuIns_2$ (p), $CuInse_2$ (p) / CdS (n) / ZnO (i) / ZnO (n) / Ni- Al. The Molybdenum (Mo) or ITO (indium tin oxide) plays the role of rear contact.

The ZnO and CdS layers are doped n by Al for ZnO and In for CdS, due to their high band gaps, they allow visible radiation to pass (hence their name of window layers) which is then absorbed in the $CuInse_2$ and $CuIns_2$ layers. The ZnO and CdS layers form the n-p junction with the $CuInSe_2$ and $CuInS_2$ layers. The buffer layer (CdS) allows the electrical and structural transition between the $CuInS_2$ / $CuInSe_2$ and ZnO. Its presence reduces the electrical losses associated with the recombination mechanisms at the interface.

2. Materials and Methods

To determine the external quantum efficiency and the resulting short-circuit photocurrent density under given solar spectrum, the optical properties of the materials will be represented by the absorption coefficients of the different layers (α_i), the purity of the materials by the diffusion length (L_{p_i}, L_{n_i}) and the diffusion coefficient (D_{p_i}, D_{n_i}) of charge carriers, the surface and interface phenomena resulting from the contacts between the materials by recombination velocities at the surface and at the interface (S_{p_i}, S_{n_i}), the solar irradiation by the corresponding photon flux (F), the geometric parameters by the thicknesses of the different layers (H_i). These various parameters are integrated into the continuity equation which governs the phenomenon of charge transport in semiconductor materials. It should be noted from these parameters that the absorption coefficient (αi) and the photon flux (F) depend on the energy of the photons (we have α_i(E) and F (E)).

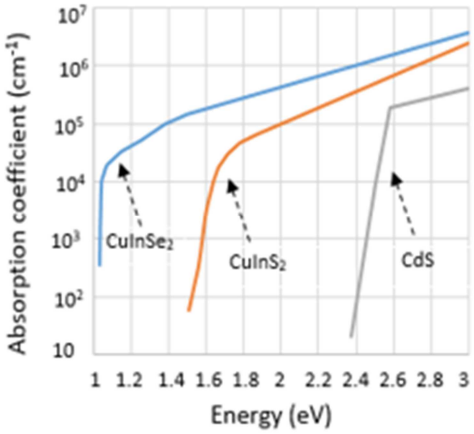

Figure 1. *Absorption coefficient of CdS, $CuInS_2$, $CuInSe_2$ materials versus photon energy [11, 23].*

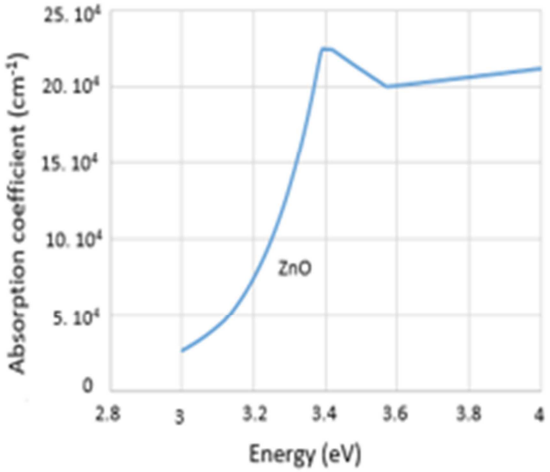

Figure 2. *Absorption coefficient of ZnO material versus photon energy [24].*

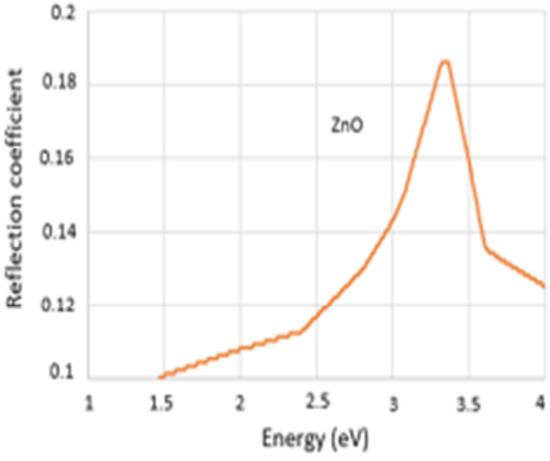

Figure 3. *Reflection coefficient of ZnO material versus photon energy [24].*

It is assumed that the optical reflection coefficient is neglected at each interface in the spectral range used. It is also considered that the space charge region is located only between the n and p regions and there is no electric field outside this region. We neglect recombination phenomena in the space charge region.

In figures 1 - 3 we represent the optical absorption coefficients of the different materials and the ZnO reflection coefficient [11, 23-24]. The diagrams of the structures are shown in figure 4.

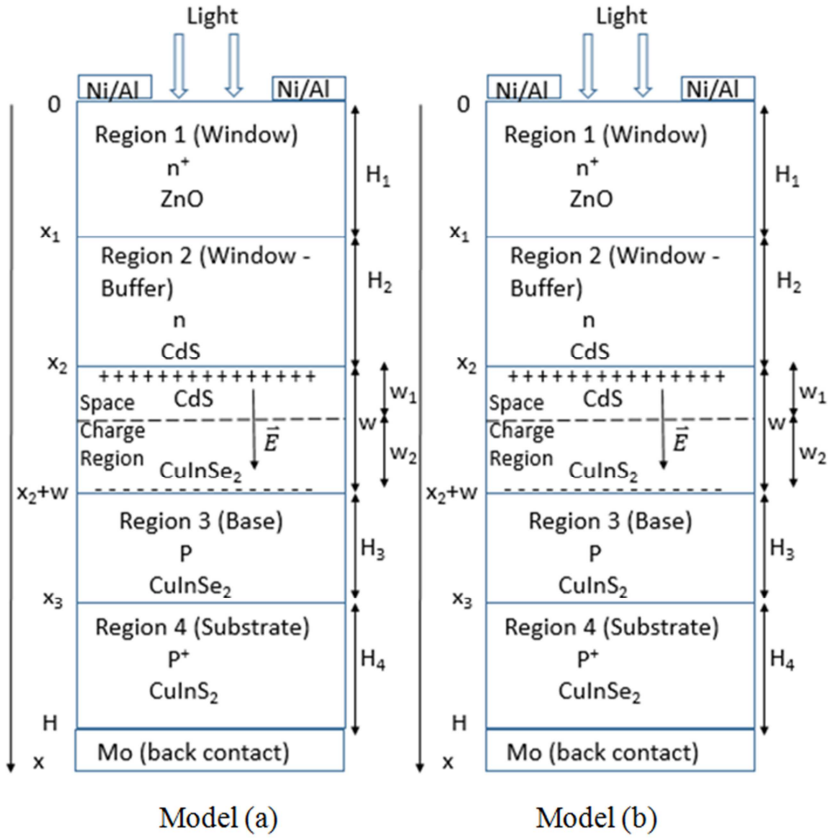

Figure 4. *Diagrams of the structures: model (a) ZnO(n^+)/CdS(n)CuInSe$_2$(p)/ CuInS$_2$(p^+); model (b) ZnO(n^+)/CdS(n)CuInS$_2$(p)/ CuInSe$_2$(p^+).*

2.1. Contribution of Region 1 on the External Quantum Efficiency

In region 1 (ZnO layer) doped n, the photocurrent is essentially due to the generated holes, the continuity equation is written as:

$$\frac{d^2\Delta p_1}{dx^2} - \frac{\Delta p_1}{{L_{p_1}}^2} = \frac{-\alpha_1 F(1-R)e^{-\alpha_1 x}}{D_{p_1}} \quad (1)$$

Basing on previous studies, boundary conditions are given as follow [18, 25].

$$D_{p_1}\left(\frac{d\Delta p_1}{dx}\right) = S_{p_1}\Delta p_1 \text{ for } x = 0 \quad (2)$$

$$\Delta p_1 = 0 \text{ for } x = x_1 \quad (3)$$

The efficiency of the collected holes which are generated in region 1 is given by:

$$\eta_{R_1} = \frac{-qD_{p_1}\frac{d\Delta p_1}{dx}\Big|_{x=x_1}}{q\,F} \quad (4)$$

It is written as:

$$\eta_{R_1} = \frac{\alpha_1(1-R)L_{p_1}}{(\alpha_1^2{L_{p_1}}^2-1)} \times \left\{\frac{\left(\frac{S_{p_1}L_{p_1}}{D_{p_1}}+\alpha_1 L_{p_1}\right) - e^{-\alpha_1 H_1}\left[\frac{S_{p_1}L_{p_1}}{D_{p_1}}ch\left(\frac{H_1}{L_{p_1}}\right)+sh\left(\frac{H_1}{L_{p_1}}\right)\right]}{\frac{S_{p_1}L_{p_1}}{D_{p_1}}sh\left(\frac{H_1}{L_{p_1}}\right)+ch\left(\frac{H_1}{L_{p_1}}\right)} - \alpha_1 L_{p_1}e^{-\alpha_1 H_1}\right\} \quad (5)$$

2.2. Contribution of Region 1 on the External Quantum Efficiency

In region 2 also doped n, the photocurrent is due to the generated holes, and results from the contribution of regions 1 and 2. The interface effects are characterized by a recombination velocity at the interface noted S_{p_2}. The continuity equation is given by:

$$\frac{d^2\Delta p_2}{dx^2} - \frac{\Delta p_2}{{L_{p_2}}^2} = \frac{-\alpha_2 F(1-R)e^{-\alpha_1 H_1}e^{-\alpha_2(x-H_1)}}{D_{p_2}} \quad (6)$$

Boundary conditions are given by previous studies as follow [25-27].

$$D_{p_2}\frac{d\Delta p_2}{dx} = S_{p_2}\Delta p_2 + D_{p_1}\frac{d\Delta p_1}{dx} \text{ for } x = x_1 \quad (7)$$

$$\Delta p_2 = 0 \text{ for } x = x_2 \quad (8)$$

The contribution of regions 1 and 2 (ZnO – CdS) to the external quantum efficiency is given by:

$$\eta_{R1-R2} = \frac{-qD_{p_2}\frac{d\Delta p_2}{dx}\Big|_{x=x_2}}{q\,F} \quad (9)$$

It is written as:

$$\eta_{R1-R2} = \frac{\alpha_2(1-R)L_{p_2}e^{-\alpha_1 H_1}}{(\alpha_2{}^2 L_{p_2}{}^2 - 1)}\left\{\frac{\left(\frac{S_{p_2}L_{p_2}}{D_{p_2}}+\alpha_2 L_{p_2}\right)}{\frac{S_{p_2}L_{p_2}}{D_{p_2}}sh\left(\frac{H_2}{L_{p_2}}\right)+ch\left(\frac{H_2}{L_{p_2}}\right)} - \frac{e^{-\alpha_2 H_2}\left[\frac{S_{p_2}L_{p_2}}{D_{p_2}}ch\left(\frac{H_2}{L_{p_2}}\right)+sh\left(\frac{H_2}{L_{p_2}}\right)\right]}{\frac{S_{p_2}L_{p_2}}{D_{p_2}}sh\left(\frac{H_2}{L_{p_2}}\right)+ch\left(\frac{H_2}{L_{p_2}}\right)} - \alpha_2 L_{p_2}e^{-\alpha_2 H_2}\right\} + \frac{\eta_{R_1}}{\frac{S_{p_2}L_{p_2}}{D_{p_2}}sh\left(\frac{H_2}{L_{p_2}}\right)+ch\left(\frac{H_2}{L_{p_2}}\right)} \quad (10)$$

2.3. Contribution of the Space Charge Region on the External Quantum Efficiency

In the space charge region, the recombination phenomena are neglected. It is formed by two areas (CdS and $CuInSe_2$ or $CuInS_2$ layers). In the first area, the thickness is fixed at w_1 (CdS) and in the second area, the thickness is fixed at w_2 ($CuInSe_2$ or $CuInS_2$). The continuity equations for the photo-created holes are written respectively as:

$$-\frac{1}{q}\frac{dJ_{w_1}}{dx} + \alpha_2 F(1-R)e^{-\alpha_1 H_1}e^{-\alpha_2(x-H_1)} = 0 \quad (11)$$

$$-\frac{1}{q}\frac{dJ_{w_2}}{dx} + \alpha_3 F(1-R)e^{-\alpha_1 H_1}e^{-\alpha_2(H_2+w_1)} \times e^{-\alpha_3[x-(H_1+H_2+w_1)]} = 0 \quad (12)$$

Boundary conditions are given by:

$$J_{w_1}(x) = 0 \text{ for } x = x_2 \quad (13)$$

$$J_{w_2}(x) = 0 \text{ for } x = x_2 + w_1 \quad (14)$$

The contribution of the space charge region (SCR) to the external quantum efficiency is given by:

$$\eta_{SCR} = \frac{J_{w_1}(x_2+w_1)+J_{w_2}(x_2+w)}{qF} \quad (15)$$

It is written as:

$$\eta_{SCR} = -(1-R)e^{-\alpha_1 H_1}\left\{e^{-\alpha_2 H_2} \times [e^{-\alpha_2 w_1} - 1] + e^{-\alpha_2(H_2+w_1)} \times [e^{-\alpha_3 w_2} - 1]\right\} \quad (16)$$

2.4. Contribution of Region 4 (Substrate) on the External Quantum Efficiency

In region 4 named substrate and doped p, the photocurrent is due to the photo-created electrons, the continuity equation is given by:

$$\frac{d^2\Delta n_4}{dx^2} - \frac{\Delta n_4}{L_{n_4}^2} = \frac{-\alpha_4}{D_{n_4}}F(1-R)e^{-\alpha_1 H_1}e^{-\alpha_2(H_2+w_1)} \times e^{-\alpha_3(H_3+w_2)}e^{-\alpha_4[x-(H-H_4)]} \quad (17)$$

Boundary conditions are given by previous studies as follow [18, 25].

$$D_{n_4}\frac{d\Delta n_4}{dx} = -S_{n_4}\Delta n_4 \text{ for } x = H \quad (18)$$

$$\Delta n_4 = 0 \text{ for } x = x_3 \quad (19)$$

The efficiency of the collected electrons which are generated in region 4 is given by:

$$\eta_{n_4} = \frac{qD_{n_4}\frac{d\Delta n_4}{dx}\Big|_{x=x_3}}{q\,F} \quad (20)$$

It is written as:

$$\eta_{n_4} = -\frac{\alpha_4 L_{n_4}(1-R)\,e^{[(\alpha_2-\alpha_1)H_1]}\,e^{[(\alpha_3-\alpha_2)(H_1+H_2+w_1)]}}{\left(\alpha_4{}^2 L_{n_4}{}^2 - 1\right)} \times e^{[(\alpha_4-\alpha_3)(H-H_4)]}$$

$$\times\left[\frac{\left(\alpha_4 L_{n_4} - \frac{S_{n_4}L_{n_4}}{D_{n_4}}\right)e^{-\alpha_4 H}}{\frac{S_{n_4}L_{n_4}}{D_{n_4}}sh\left(\frac{H_4}{L_{n_4}}\right)+ch\left(\frac{H_4}{L_{n_4}}\right)} + \frac{e^{-\alpha_4(H-H_4)}\left[\frac{S_{n_4}L_{n_4}}{D_{n_4}}\cdot\mathrm{ch}\left(\frac{H_4}{L_{n_4}}\right)+\mathrm{sh}\left(\frac{H_4}{L_{n_4}}\right)\right]}{\frac{S_{n_4}L_{n_4}}{D_{n_4}}sh\left(\frac{H_4}{L_{n_4}}\right)+ch\left(\frac{H_4}{L_{n_4}}\right)} - \alpha_4 L_{n_4}e^{-\alpha_4(H-H_4)}\right] \quad (21)$$

2.5. Contribution of Region 3 (Base) on the External Quantum Efficiency

In region 3 named base and doped p, the photocurrent is due to the generated electrons. The continuity equation is given by:

$$\frac{d^2\Delta n_3}{dx^2} - \frac{\Delta n_3}{L_{n_3}^2} = \frac{-\alpha_3}{D_{n_3}} F(1-R) e^{-\alpha_1 H_1} e^{-\alpha_2 (H_2+w_1)} \times e^{-\alpha_3 [x-(H_1+H_2+w_1)]} \quad (22)$$

Basing on previous studies, boundary conditions can be written as [10, 28].

$$\Delta n_3 = 0 \text{ for } x = x_2 + w \quad (23)$$

$$D_{n_3} \frac{d\Delta n_3}{dx} = -S_{n_3} \Delta n_3 + D_{n_4} \frac{d\Delta n_4}{dx} \text{ for } x = x_3 \quad (24)$$

The contribution of regions 3 and 4 (base – substrate) to the external quantum efficiency is given by:

$$\eta_{R3-R4} = \frac{q D_{n_3} \frac{d\Delta n_3}{dx}\Big|_{x=x_2+w}}{qF} \quad (25)$$

It is written as:

$$\eta_{R3-R4} = -\frac{\alpha_3 L_{n_3}(1-R)\, e^{[(\alpha_2-\alpha_1)H_1]}}{(\alpha_3{}^2 L_{n_3}{}^2 - 1)} \times e^{[(\alpha_3-\alpha_2)(H_1+H_2+w_1)]} \left[\frac{\left(\alpha_3 L_{n_3} - \frac{S_{n_3} L_{n_3}}{D_{n_3}}\right) e^{-\alpha_3 (H-H_4)}}{\frac{S_{n_3} L_{n_3}}{D_{n_3}} sh\left[\frac{H_3}{L_{n_3}}\right] + ch\left[\frac{H_3}{L_{n_3}}\right]} + \frac{e^{-\alpha_3 (H_1+H_2+w)} \left[\frac{S_{n_3} L_{n_3}}{D_{n_3}} \cdot \text{ch}\left(\frac{H_3}{L_{n_3}}\right) + \text{sh}\left(\frac{H_3}{L_{n_3}}\right)\right]}{\frac{S_{n_3} L_{n_3}}{D_{n_3}} sh\left[\frac{H_3}{L_{n_3}}\right] + ch\left[\frac{H_3}{L_{n_3}}\right]} - \alpha_3 L_{n_3} e^{-\alpha_3 (H_1+H_2+w)} \right] + \frac{\eta_{n_4}}{\frac{S_{n_3} L_{n_3}}{D_{n_3}} sh\left[\frac{H_3}{L_{n_3}}\right] + ch\left[\frac{H_3}{L_{n_3}}\right]} \quad (26)$$

2.6. Total External Quantum Efficiency

The total external quantum efficiency EQE is the sum of the contributions of the different regions on the efficiency, it is given by:

$$\text{EQE} = \eta_{R1-R2} + \eta_{SCR} + \eta_{R3-R4} \quad (27)$$

3. Results and Discussion

The values of the standard parameters used for the modeling are indicated in the following table 1:

Table 1. *Physical standard parameters considered.*

Model (a) & Model (b)	
H_1 = 0.3 µm	H_3 = 1 µm
Lp_1= 0.3 µm	Ln_3 = 3 µm
$Sp_1 = 2.10^7$ cm.s^{-1}	$Sn_3 = 2.10^5$ cm.s^{-1}
Dp_1 = 0.51 cm^2.s^{-1}	Dn_3 = 5.13 cm^2.s^{-1}
H_2 = 0.1 µm	H_4 = 98.5 µm
Lp_2 = 0.4 µm	Ln_4 = 1 µm
$Sp_2 = 2.10^5$ cm.s^{-1}	$Sn_4 = 2.10^7$ cm.s^{-1}
Dp_2 = 0.64 cm^2.s^{-1}	Dn_4 = 10.27 cm^2.s^{-1}
W_1 = 0.02 µm	W_2 = 0.08 µm

Figure 5 shows the contribution of each region of the photovoltaic structure on the resulting external quantum efficiency (EQE) for the models (a) and (b).

3.1. Solar Spectra and External Quantum Efficiency

Figure 6 shows the definition of the air-mass (AM) standard [29]. Figure 7 represents the photon fluxes which correspond to the three reference solar spectra AM0, AM1, AM1.5 versus the wavelength, they are adapted from [30]. They correspond to respective irradiations of 1353 W.m^{-2}, 931 W.m^{-2}, 834 W.m^{-2} [29-30]. Figure 8 shows the comparison of the external quantum efficiency (EQE) of the two models (a) and (b) versus the wavelength, it is obtained using equation (27). We note that the solar cells are sensitive to the spectrum ranging from near infrared to visible. To determine by numerical method the short-circuit photocurrent density which corresponds to the maximum current density of the solar cell, we used the values of tables 1 and 9. Table 1 indicates the values of the parameters used for the modeling and table 9 indicates the discretized values of the energy, the wavelength, the photon fluxes and the external quantum efficiency. Table 9 is indicated in Appendix.

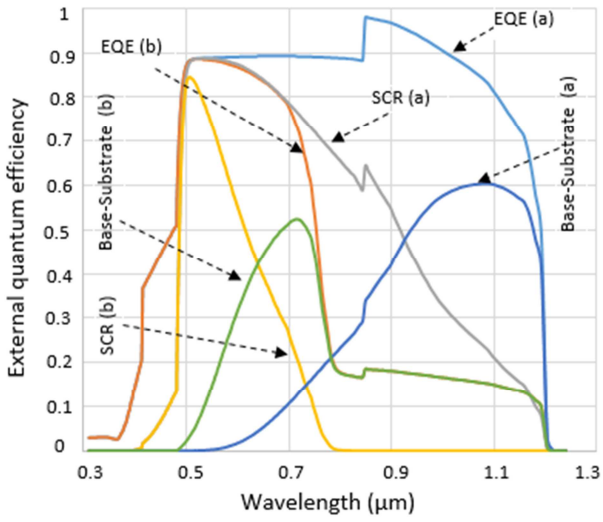

Figure 5. *Contribution of the different regions of the solar cell to the external quantum efficiency vs. photon wavelength for each model.*

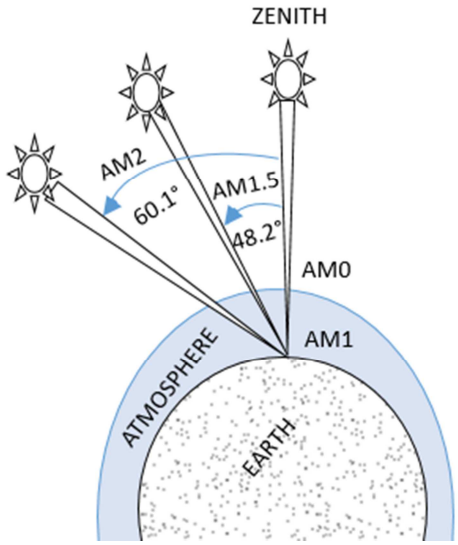

Figure 6. *Definition of the AM standard [29].*

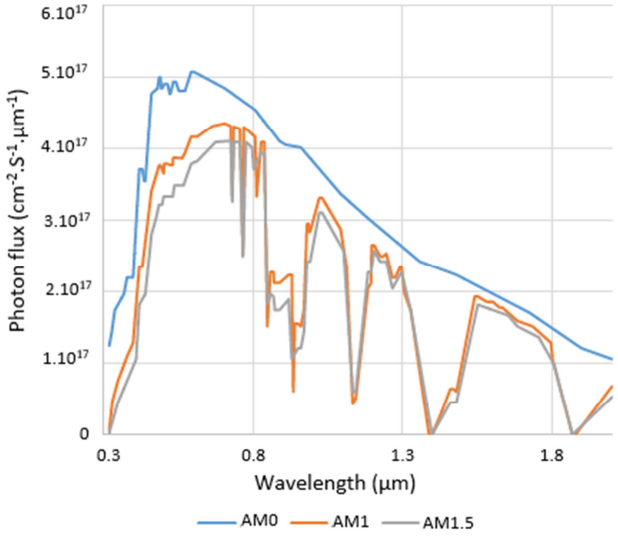

Figure 7. *Photon flux vs. photon wavelength [30].*

In model (b) $ZnO(n^+)/CdS(n)/CuInS_2(p)/CuInSe_2(p^+)$, the materials are arranged by decreasing energy band gap, the external quantum efficiency depends on the responses of the different layers of the structure. Since the spectral response begins with the photon absorption by the smaller energy band gap materials, the back layers absorb at first incident photons (substrate → base → space charge region → window layers).

In model (a) $ZnO(n^+)/CdS(n)/CuInSe_2(p)/CuInS_2(p^+)$, materials are not arranged with a decreasing energy band gap. The base ($CuInSe_2$) has the smallest energy band gap and a high photon absorption coefficient, it absorbs at first the incident photons and reduces substrate contribution (base → space charge region → substate → window layers). This model has the greatest external quantum efficiency for the same standard parameters considered of the two structures indicated in table 1. This difference in efficiency of the two models differentiated just by the position of the materials shows the importance of the contribution of the base and the space charge region.

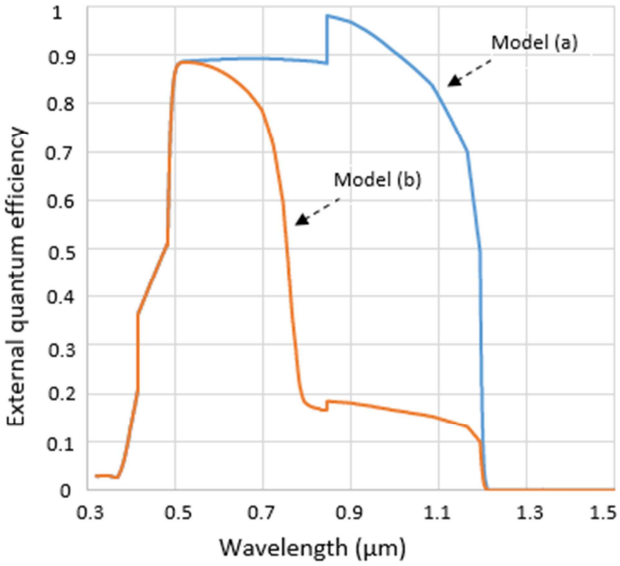

Figure 8. *External quantum efficiency vs. photon wavelength: comparison between model (a) and model (b).*

The difference between models (a) and (b) is that with model (b) we can avoid the generation of hot carriers by placing the gaps of materials in a decreasing manner while with model (a) favors the generation of these carriers. Hot carriers are carriers generated by photons having an energy greater than the gap of the material, they pass from the valence band above the minimum of the conduction band. These carriers can participate in the phenomenon of electrical conduction only after losing their excess energy by thermalization to pass to the minimum of the conduction band where they can participate in the external quantum efficiency if they have a sufficient diffusion length. However, we specify that the influence of hot carriers on the external quantum efficiency is not taken into account by the computational model used.

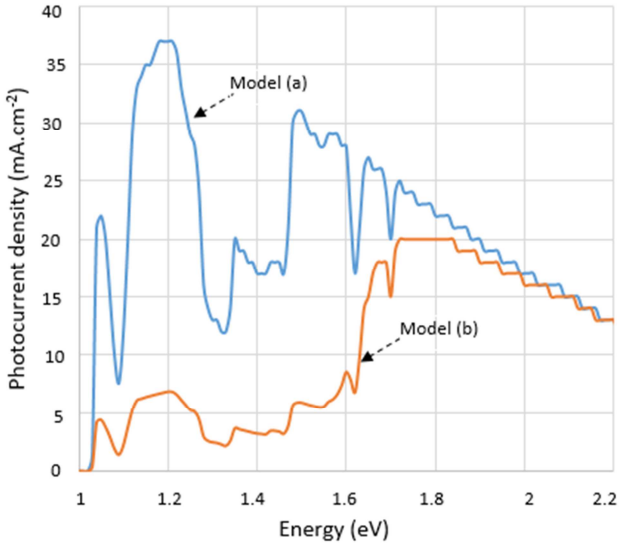

Figure 9. *Resulting photocurrent density vs. photon energy under polychromatic illumination for AM1.5 solar spectrum.*

In figure 9 we represent, under the spectrum AM1.5, the resulting photocurrent density $J_{ph}(E)$ versus photon energy. It is expressed in A.cm^{-2}.eV^{-1}. To draw this graph we have used the relations (28)-(31).

$$J_{ph}(E) = q\ F\ (E)\ \text{EQE (E)} \tag{28}$$

$$\lambda\ (\mu m) = \frac{1.24}{E\ (eV)} \tag{29}$$

$$F\ (E) = \Phi(\lambda) \times \frac{1.24}{E^2} \tag{30}$$

$$J_{ph}(E) = q\ \Phi(\lambda) \times \frac{1.24}{E^2}\ \text{EQE (E)} \tag{31}$$

$\Phi(\lambda)$ represents the flux of photons versus the wavelength (figure 7), it is expressed in cm^{-2}.s^{-1}.µm^{-1}. $F\ (E)$ is the flux of photons versus the energy, it expressed in cm^{-2}.s^{-1}.eV^{-1}. The relations between $\Phi(\lambda)$ and $F\ (E)$ are given by the equations (29) and (30). The wavelength λ is expressed in µm and the energy E in eV.

Calculation of the short-circuit photocurrent density J_{sc} on the solar spectral ranging from 1 eV to 4 eV is given by the expression (32). For this calculation, we propose a numerical integration method and use the Newton quadrature.

$$J_{sc} = \int_1^4 J_{ph}\ (E)dE \approx \frac{\delta E}{2}\begin{bmatrix} J_{ph}(E_1) + J_{ph}(E_{m+1}) + \\ 2\sum_{i=2}^{m} J_{ph}(E_i) \end{bmatrix} \tag{32}$$

By replacing $J_{ph}(E)$ by the expression (31) we obtain:

$$J_{sc} = \int_1^4 J_{ph}\ (E)dE \approx \frac{\delta E}{2}\left[q\ \Phi(E_1) \times \frac{1.24}{E_1^2}\ \text{EQE}\ (E_1) + q\ \Phi(E_{m+1}) \times \frac{1.24}{E_{m+1}^2}\ \text{EQE}\ (E_{m+1}) + 2\sum_{i=2}^{m} q\ \Phi(E_i) \times \frac{1.24}{E_i^2}\ \text{EQE}\ (E_i)\right] \tag{33}$$

With: $E \in [1, 4]$;
$E_{i+1} = E_1 + i \cdot \delta E$ with: $i: 1 \ldots m$

$$\delta E = \frac{E_{m+1} - E_1}{m}$$

We have taken for this calculation:

$$E_1 = 1\ eV;\ E_{m+1} = 3.88\ eV;\ \delta E = 0.03\ eV;\ m\ = 96$$

Using table 9 and equation (33) we obtain the following short-circuit photocurrent density established in table 2 for the three solar spectra AM0, AM1, AM1.5.

Table 2. *Short-circuit photocurrent density.*

	AM0	AM1	AM1.5
Model (a)	*44.92 mA.cm^{-2}*	*33.031 mA.cm^{-2}*	*30.179 mA.cm^{-2}*
Model (b)	*24.525 mA.cm^{-2}*	*19.309 mA.cm^{-2}*	*17.507 mA.cm^{-2}*

The short-circuit photocurrent density depends on the parameters considered. Tables 3 - 8 show its evolution by varying the values of certain parameters such as diffusion length, thickness and recombination velocity. We can observe that the Optimization of parameters during growth of materials is essential to obtain better photocurrent.

3.2. Effect of Parameters

However, in this part we show that the external quantum efficiency or the collected photo-current can be improved in the model (b) and also in the model (a), by making an adequate dimensioning which is according to the considered structure. For that we will study the evolution of the short-circuit photocurrent density according to the variation of each parameter (thickness, diffusion length, recombination velocity) of the rear area which is essentially responsible to the spectral response (substrate, base and space charge region) as the front plays the role of window layer. Then we determine the optimal parameters for each model that gives the greatest performance. A comparative diagram is then done to compare the evolution of the current collected according to the considered parameters of each model.

3.2.1. Effect of Base Thickness

The figure 10 shows the base-substrate response for each model. The wavelength range greater than 0.8 µm models the absorption of $CuInSe_2$ layer used as a base in model (a) and used as a substrate in model (b). The wavelength range between 0.5 to 0.8 µm shows the absorption of $CuInS_2$ layer used as a substrate in model (a) and as a base in model (b). The decay of each curve models the absorption of photons by the space charge region and the front area. For the wavelength range less than 0.5 µm no photons access the base.

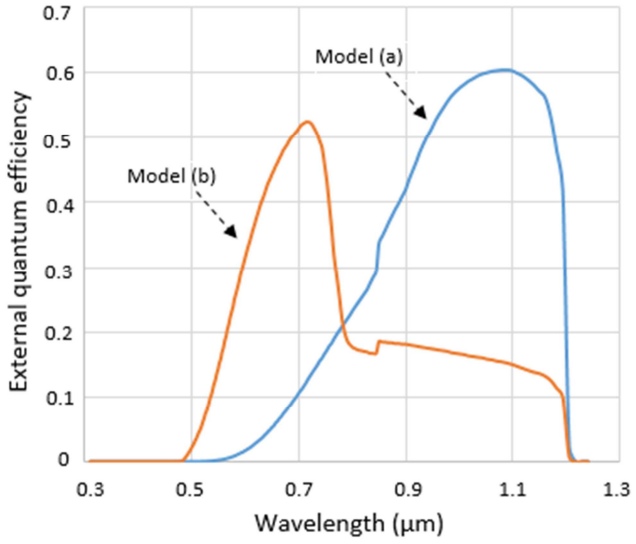

Figure 10. *Base and Substrate response for models (a) and (b) vs. photon wavelength.*

Table 3. *Short-circuit photocurrent density for optimized base thickness.*

Model (a)		**Model (b)**	
Region 1	Region 3	Region 1	Region 3
$H_1 = 0.3$ µm	$H_3 = 6$ µm	$H_1 = 0.3$ µm	$H_3 = 0.1$ µm
$Lp_1 = 0.3$ µm	$Ln_3 = 3$ µm	$Lp_1 = 0.3$ µm	$Ln_3 = 3$ µm
$Sp_1 = 2.10^7$ cm.s^{-1}	$Sn_3 = 2.10^5$ cm.s^{-1}	$Sp_1 = 2.10^7$ cm.s^{-1}	$Sn_3 = 2.10^5$ cm.s^{-1}
$Dp_1 = 0.51$ cm^2.s^{-1}	$Dn_3 = 5.13$ cm^2.s^{-1}	$Dp_1 = 0.51$ cm^2.s^{-}	$Dn_3 = 5.13$ cm^2.s^{-1}
Region 2	Region 4	Region 2	Region 4
$H_2 = 0.1$ µm	$H_4 = 98.5$ µm	$H_2 = 0.1$ µm	$H_4 = 98.5$ µm
$Lp_2 = 0.4$ µm	$Ln_4 = 1$ µm	$Lp_2 = 0.4$ µm	$Ln_4 = 1$ µm
$Sp_2 = 2.10^5$ cm.s^{-1}	$Sn_4 = 2.10^7$ cm.s^{-1}	$Sp_2 = 2.10^5$ cm.s^{-1}	$Sn_4 = 2.10^7$ cm.s^{-1}
$Dp_2 = 0.64$ cm^2.s^{-1}	$Dn_4 = 10.27$ cm^2.s^{-1}	$Dp_2 = 0.64$ cm^2.s^{-1}	$Dn_4 = 10.27$ cm^2.s^{-1}
SCR 1	SCR 2	SCR 1	SCR 2
$W_1 = 0.02$ µm	$W_2 = 0.08$ µm	$W_1 = 0.02$ µm	$W_2 = 0.08$ µm

Spectrum	**Photocurrent**	**Spectrum**	**Photocurrent**
AM0	Jsc = 46.562 mA.cm^{-2}	AM0	Jsc = 35.43 mA.cm^{-2}
AM1	Jsc = 34.085 mA.cm^{-2}	AM1	Jsc = 26.409 mA.cm^{-2}
AM1.5	Jsc = 31.181 mA.cm^{-2}	AM1.5	Jsc = 24.058 mA.cm^{-2}

Figure 11 represents the evolution of the short-circuit photocurrent density versus the thickness of the base. For model (a) the photocurrent increases with the thickness and tends to a constant value from a certain value of the thickness. In fact, in this model, since the gap of the base is smaller than that of the substrate, the photons hardly reach the substrate; they are all practically absorbed by the base. The contribution of this region increases with thickness.

Contrary to the model (a), in model (b) the photocurrent increases by reducing the thickness of the base. In this model the carriers reach the substrate since the gap of the base is greater than that of the substrate. The contribution of the substrate increases by decreasing the thickness of the base, this reduction allows the carrier generated in the substrate to reach the space charge zone by covering less distance.

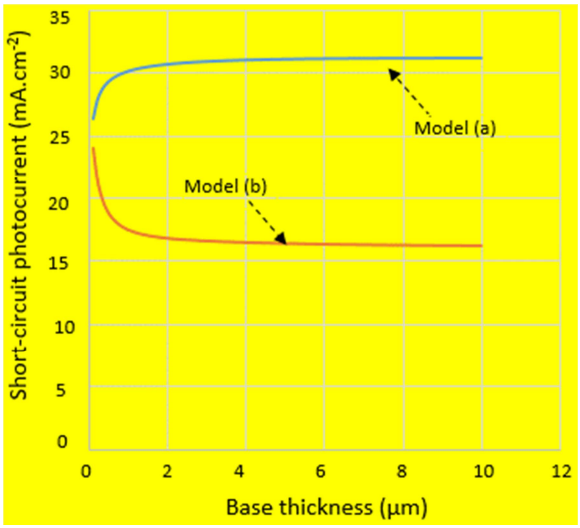

Figure 11. *Evolution of the photocurrent for models (a) and (b) vs. thickness of the base.*

Thus the optimization of the base thickness depends on the structure of the cell, for model (a) it suffices to increase the thickness and for model (b) to reduce it.

Based on table 1 we will optimize the various parameters by studying the evolution of the photocurrent according to each considered parameter. Table 3 indicates the evolution of the value of the short-circuit photocurrent density for optimal thicknesses set at 6 µm for the model (a) and 0.1 µm for the model (b).

3.2.2. Effect of Space Charge Region Thickness

Figure 12 represents the contribution of the space charge region for each model. Model (a) gives a higher contribution compared to model (b) and has a wider absorption spectrum in this area. Indeed this is explained by the fact that in the space charge region, the absorption is due by the $CuInSe_2$ for the model (a) and by the $CuInS_2$ for the model (b). $CuInSe_2$ has a larger absorption and a higher absorption coefficient allowing to generate more electron hole pairs compared to $CuInS_2$. In the space charge region, the losses are neglected, all carriers generated in this area are supposed to be collected.

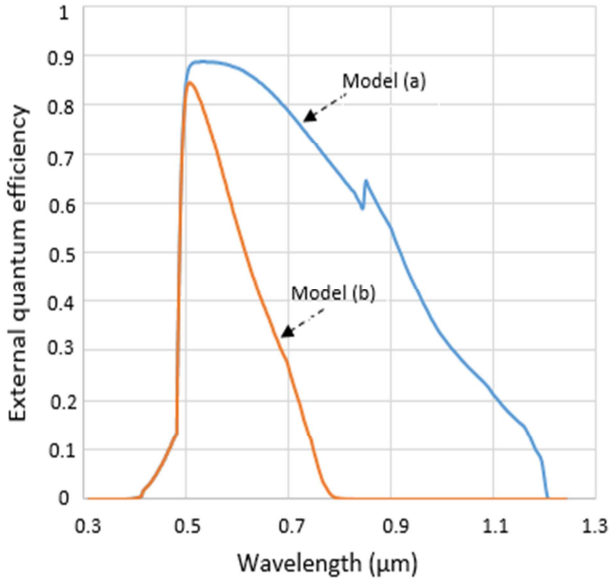

Figure 12. *Space charge region response for models (a) and (b) vs. photon wavelength.*

Table 4. *Short-circuit photocurrent density for optimized space charge region thickness.*

Model (a)		**Model (b)**	
Region 1	Region 3	Region 1	Region 3
H_1 = 0.3 µm	H_3 = 1 µm	H_1 = 0.3 µm	H_3 = 1 µm
Lp_1= 0.3 µm	Ln_3 = 3 µm	Lp_1= 0.3 µm	Ln_3 = 3 µm
$Sp_1 = 2.10^7$ cm.s^{-1}	$Sn_3 = 2.10^5$ cm.s^{-1}	$Sp_1 = 2.10^7$ cm.s^{-1}	$Sn_3 = 2.10^5$ cm.s^{-1}
Dp_1 = 0.51 cm^2.s^{-1}	Dn_3 = 5.13 cm^2.s^{-1}	Dp_1 = 0.51 cm^2.s$^-$	Dn_3 = 5.13 cm^2.s^{-1}
Region 2	Region 4	Region 2	Region 4
H_2 = 0.1 µm	H_4 = 98.5 µm	H_2 = 0.1 µm	H_4 = 98.5 µm
Lp_2 = 0.4 µm	Ln_4 = 1 µm	Lp_2 = 0.4 µm	Ln_4 = 1 µm
$Sp_2 = 2.10^5$ cm.s^{-1}	$Sn_4 = 2.10^7$ cm.s^{-1}	$Sp_2 = 2.10^5$ cm.s^{-1}	$Sn_4 = 2.10^7$ cm.s^{-1}
Dp_2 = 0.64 cm^2.s^{-1}	Dn_4 = 10.27 cm^2.s^{-1}	Dp_2 = 0.64 cm^2.s^{-1}	Dn_4 = 10.27 cm^2.s^{-1}
SCR 1	SCR 2	SCR 1	SCR 2
W_1 = 0.02 µm	W_2 = 1 µm	W_1 = 0.02 µm	W_2 = 1 µm

Spectrum	**Photocurrent**	**Spectrum**	**Photocurrent**
AM0	Jsc = 47.372 mA.cm^{-2}	AM0	Jsc = 26.298 mA.cm^{-2}
AM1	Jsc = 34.563 mA.cm^{-2}	AM1	Jsc = 20.855 mA.cm^{-2}
AM1.5	Jsc = 31.633 mA.cm^{-2}	AM1.5	Jsc = 18.929 mA.cm^{-2}

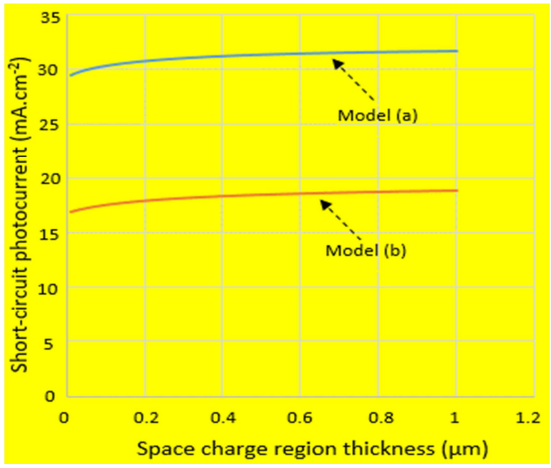

Figure 13. *Evolution of the photocurrent for models (a) and (b) vs. thickness of the space charge region.*

Figure 13 shows for each model the evolution of the short-circuit photocurrent density versus the thickness of the space charge region, the photocurrent increases by increasing the thickness of the space charge region. Thus, table 4 indicates the evolution of the value of the photocurrent for an optimum thickness of the space charge region set at 1 µm in the absorption areas of $CuInSe_2$ and $CuInS_2$ (SCR2) for each model. It should be noted that the increase in the thickness of the space charge region is done by reducing the doping rate which could favor the cancellation of the photocurrent for a low forward bias voltage.

3.2.3. Effect of Diffusion Length in the Base

Figure 14 shows the evolution of the short-circuit photocurrent density versus the diffusion length in the base, the current increases with this parameter and becomes constant from a certain value of the diffusion length. We can notice the influence of the diffusion length much more in the model (b) compared to the model (a). The evolution of the photocurrent is indicated in table 5 for an optimal diffusion length set at 10 µm for each model.

Table 5. *Short-circuit photocurrent density for optimized diffusion length in the base.*

Model (a)		**Model (b)**	
Region 1	Region 3	Region 1	Region 3
H_1 = 0.3 µm	H_3 = 1 µm	H_1 = 0.3 µm	H_3 = 1 µm
Lp_1= 0.3 µm	Ln_3 = 10 µm	Lp_1= 0.3 µm	Ln_3 = 10 µm
$Sp_1 = 2.10^7$ cm.s^{-1}	$Sn_3 = 2.10^5$ cm.s^{-1}	$Sp_1 = 2.10^7$ cm.s^{-1}	$Sn_3 = 2.10^5$ cm.s^{-1}
Dp_1 = 0.51 cm^2.s^{-1}	Dn_3 = 5.13 cm^2.s^{-1}	Dp_1 = 0.51 cm^2.s$^-$	Dn_3 = 5.13 cm^2.s^{-1}
Region 2	Region 4	Region 2	Region 4
H_2 = 0.1 µm	H_4 = 98.5 µm	H_2 = 0.1 µm	H_4 = 98.5 µm
Lp_2 = 0.4 µm	Ln_4 = 1 µm	Lp_2 = 0.4 µm	Ln_4 = 1 µm
$Sp_2 = 2.10^5$ cm.s^{-1}	$Sn_4 = 2.10^7$ cm.s^{-1}	$Sp_2 = 2.10^5$ cm.s^{-1}	$Sn_4 = 2.10^7$ cm.s^{-1}
Dp_2 = 0.64 cm^2.s^{-1}	Dn_4 = 10.27 cm^2.s^{-1}	Dp_2 = 0.64 cm^2.s^{-1}	Dn_4 = 10.27 cm^2.s^{-1}
SCR 1	SCR 2	SCR 1	SCR 2
W_1 = 0.02 µm	W_2 = 0.08 µm	W_1 = 0.02 µm	W_2 = 0.08 µm

Spectrum	**Photocurrent**	**Spectrum**	**Photocurrent**
AM0	Jsc = 45.007 mA.cm^{-2}	AM0	Jsc = 24.669 mA.cm^{-2}
AM1	Jsc = 33.086 mA.cm^{-2}	AM1	Jsc = 19.413 mA.cm^{-2}
AM1.5	Jsc = 30.23 mA.cm^{-2}	AM1.5	Jsc = 17.603 mA.cm^{-2}

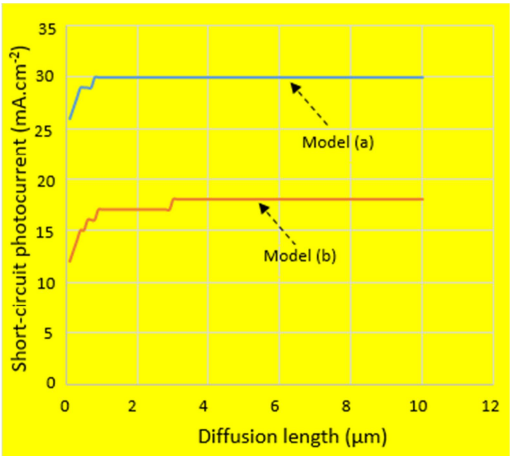

Figure 14. *Evolution of the photocurrent for models (a) and (b) vs. the diffusion length in the base.*

3.2.4. Effect of Base/Substrate Recombination Velocity

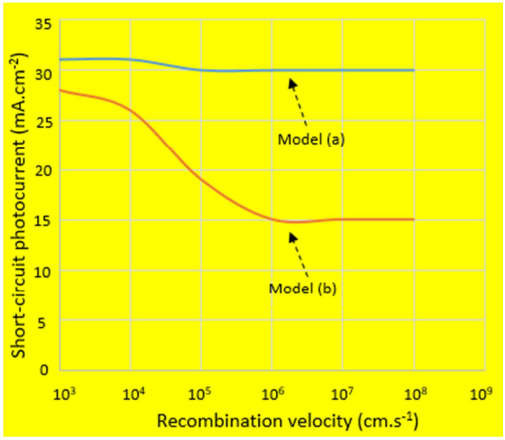

Figure 15. *Evolution of the photocurrent for models (a) and (b) vs. recombination velocity at the base-substrate interface.*

Figure 15 shows the evolution of the short-circuit photocurrent density versus the recombination velocity at the base-substrate interface; we notice that the recombination velocity has little influence on the photocurrent in model (a), this is explained by the fact that in this model the carriers are not generated near the base-substrate interface, the carriers are largely generated from the space charge region and in a low thickness of the base due to the high absorption coefficient of the $CuInSe_2$ absorbent layer.

For model (b) the recombination velocity at the base-substrate interface influences the photocurrent much more compared to model (a). The current reaches its maximum value and becomes quasi-constant for values of the recombination velocity lower than 2.10^3 $cm.s^{-1}$, the photocurrent decreases for recombination velocity values greater than 2.10^3 $cm.s^{-1}$ then reaches its minimum value and becomes quasi-constant for recombination velocity values greater than 2.10^6 $cm.s^{-1}$. The influence of the recombination velocity on the photocurrent is explained by the absorption of photons by the substrate because this structure has a decreasing band gap, these carriers must cross the interface to reach the space charge region. Also, the absorption coefficient of $CuInS_2$ constituting the space charge region and the base is lower than that of $CuInSe_2$, the carriers are generated more in depth and are more subject to the influence of the interface. In table 6 we indicate the evolution of the current for an optimal value of the recombination velocity set at 2.10^3 $cm.s^{-1}$ for the two models.

Table 6. *Short-circuit photocurrent density for optimized recombination velocity at the base-substrate interface.*

	AM0	**AM1**	**AM1.5**
Model (a)	*46.644 mA.cm^{-2}*	*34.116 mA.cm^{-2}*	*31.202 mA.cm^{-2}*
Model (b)	*41.371 mA.cm^{-2}*	*30.671 mA.cm^{-2}*	*28.003 mA.cm^{-2}*

3.2.5. Optimization of All Parameters

In Table 7 we present the results for the optimization of all parameters in the base and the substrate. In table 8 we present the results for the optimization of all parameters in the space charge region, in the base and the substrate. The evolution of the results of tables 2 – 8, is represented in histogram and graph forms in figures 16 and 17 respectively.

Table 7. *Short-circuit photocurrent density for optimized parameters in the base and the substrate.*

Model (a)		**Model (b)**	
Region 1	Region 3	Region 1	Region 3
$H_1 = 0.3$ µm	$H_3 = 6$ µm	$H_1 = 0.3$ µm	$H_3 = 0.1$ µm
$Lp_1 = 0.3$ µm	$Ln_3 = 10$ µm	$Lp_1 = 0.3$ µm	$Ln_3 = 10$ µm
$Sp_1 = 2.10^7$ $cm.s^{-1}$	$Sn_3 = 2.10^3$ $cm.s^{-1}$	$Sp_1 = 2.10^7$ $cm.s^{-1}$	$Sn_3 = 2.10^3$ $cm.s^{-1}$
$Dp_1 = 0.51$ $cm^2.s^{-1}$	$Dn_3 = 5.13$ $cm^2.s^{-1}$	$Dp_1 = 0.51$ $cm^2.s^{-}$	$Dn_3 = 5.13$ $cm^2.s^{-1}$
Region 2	Region 4	Region 2	Region 4
$H_2 = 0.1$ µm	$H_4 = 98.5$ µm	$H_2 = 0.1$ µm	$H_4 = 98.5$ µm
$Lp_2 = 0.4$ µm	$Ln_4 = 5$ µm	$Lp_2 = 0.4$ µm	$Ln_4 = 5$ µm
$Sp_2 = 2.10^5$ $cm.s^{-1}$	$Sn_4 = 2.10^7$ $cm.s^{-1}$	$Sp_2 = 2.10^5$ $cm.s^{-1}$	$Sn_4 = 2.10^7$ $cm.s^{-1}$
$Dp_2 = 0.64$ $cm^2.s^{-1}$	$Dn_4 = 10.27$ $cm^2.s^{-1}$	$Dp_2 = 0.64$ $cm^2.s^{-1}$	$Dn_4 = 10.27$ $cm^2.s^{-1}$
SCR 1	SCR 2	SCR 1	SCR 2
$W_1 = 0.02$ µm	$W_2 = 0.08$ µm	$W_1 = 0.02$ µm	$W_2 = 0.08$ µm

Spectrum	**Photocurrent**	**Spectrum**	**Photocurrent**
AM0	Jsc = 47.815 mA.cm^{-2}	AM0	Jsc = 46.779 mA.cm^{-2}
AM1	Jsc = 34.944 mA.cm^{-2}	AM1	Jsc = 34.249 mA.cm^{-2}
AM1.5	Jsc = 31.989 mA.cm^{-2}	AM1.5	Jsc = 31.338 mA.cm^{-2}

Table 8. *Short-circuit photocurrent density for optimized parameters in the space charge region, the base and the substrate.*

Model (a)		**Model (b)**	
Region 1	Region 3	Region 1	Region 3
H_1 = 0.3 µm	H_3 = 6 µm	H_1 = 0.3 µm	H_3 = 0.1 µm
Lp_1= 0.3 µm	Ln_3 = 10 µm	Lp_1= 0.3 µm	Ln_3 = 10 µm
$Sp_1 = 2.10^7$ cm.s^{-1}	$Sn_3 = 2.10^3$ cm.s^{-1}	$Sp_1 = 2.10^7$ cm.s^{-1}	$Sn_3 = 2.10^3$ cm.s^{-1}
Dp_1 = 0.51 cm^2.s^{-1}	Dn_3 = 5.13 cm^2.s^{-1}	Dp_1 = 0.51 cm^2.s^{-}	Dn_3 = 5.13 cm^2.s^{-1}
Region 2	Region 4	Region 2	Region 4
H_2 = 0.1 µm	H_4 = 98.5 µm	H_2 = 0.1 µm	H_4 = 98.5 µm
Lp_2 = 0.4 µm	Ln_4 = 5 µm	Lp_2 = 0.4 µm	Ln_4 = 5 µm
$Sp_2 = 2.10^5$ cm.s^{-1}	$Sn_4 = 2.10^7$ cm.s^{-1}	$Sp_2 = 2.10^5$ cm.s^{-1}	$Sn_4 = 2.10^7$ cm.s^{-1}
Dp_2 = 0.64 cm^2.s^{-1}	Dn_4 = 10.27 cm^2.s^{-1}	Dp_2 = 0.64 cm^2.s^{-1}	Dn_4 = 10.27 cm^2.s^{-1}
SCR 1	SCR 2	SCR 1	SCR 2
W_1 = 0.02 µm	W_2 = 1 µm	W_1 = 0.02 µm	W_2 = 1 µm

Spectrum	**Photocurrent**	**Spectrum**	**Photocurrent**
AM0	Jsc = 48.119 mA.cm^{-2}	AM0	Jsc = 46.841 mA.cm^{-2}
AM1	Jsc = 35.155 mA.cm^{-2}	AM1	Jsc = 34.303 mA.cm^{-2}
AM1.5	Jsc = 32.188 mA.cm^{-2}	AM1.5	Jsc = 31.388 mA.cm^{-2}

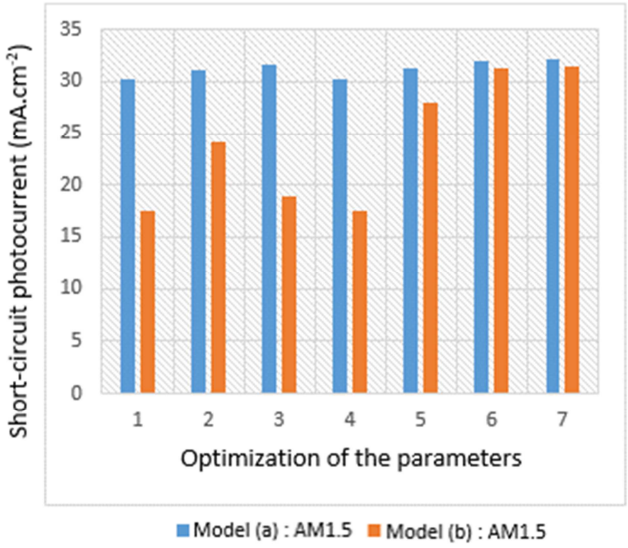

Figure 16. *Bar histogram of the photocurrent for models (a) and (b) vs. the optimization of the parameters for the AM1.5 spectrum.*

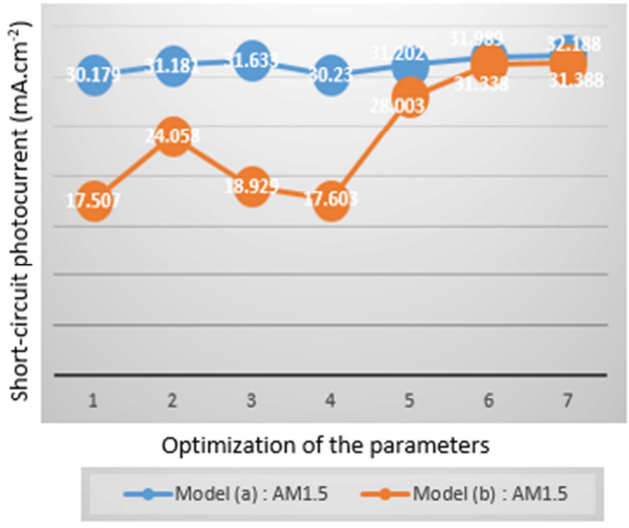

Figure 17. *Evolution graph of the photocurrent for models (a) and (b) vs. the optimization of the parameters for the AM1.5 spectrum.*

(1) standard parameters;
(2) optimization of the base thickness;
(3) optimization of the space charge region thickness;
(4) optimization of the diffusion length in the base;
(5) optimization of the recombination velocity at the base-substrate interface;
(6) optimization of the parameters in the base and the substrate;
(7) optimization of the parameters in the space charge region, the base and the substrate.

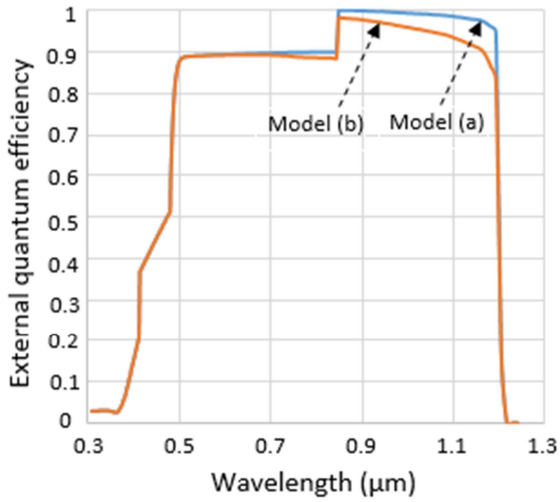

Figure 18. *Evolution of the external quantum efficiency for models (a) and (b) vs. photon wavelength.*

Figures 16 and 17 represent the evolution of the short-circuit photocurrent density according to the optimization of the parameters for the AM1.5 spectrum.

For model (b) the optimization of all parameters gives the largest short-circuit current (31.338 mA.cm^{-2} and 31.388 mA.cm^{-2}), followed respectively by the optimization of the recombination velocity at the base-substrate interface (28.003 mA.cm^{-2}), the optimization of base thickness (24.058 mA.cm^{-2}), the optimization of space charge region thickness (18.929 mA.cm^{-2}) and the optimization of diffusion length

(17.603 mA.cm^{-2}).

Regarding model (a) the optimization of all parameters gives the largest short-circuit current (31.989 mA.cm^{-2} and 32.188 mA.cm^{-2}), followed respectively by the optimization of space charge region thickness (31.633 mA.cm^{-2}), the optimization of the recombination velocity at the base-substrate interface (31.202 mA.cm^{-2}), the optimization of base thickness (31.181 mA.cm^{-2}) and the optimization of diffusion length (30.23 mA.cm^{-2}). Thus the optimization parameters depend on the structure of the cell (juxtaposition of the layers).

Figure 18 shows the evolution of the external quantum efficiency for the optimized parameters in the base and the substrate, we note an improvement in the efficiency of model (b) whose spectral response curve is substantially equal to that of model (a).

4. Conclusion

In this work, we studied the performance evolution of photovoltaic cells by optimizing some parameters of photoconductive layers. Two models are considered, ZnO(n$^+$)/CdS(n)/CuInSe$_2$(p)/CuInS$_2$(p$^+$) named model (a) and ZnO(n$^+$)/CdS(n)/CuInS$_2$(p)/CuInSe$_2$(p$^+$) named model (b). To show the importance of the optimization of parameters, the evolution of the performance of these solar cells was studied by gradually varying the thicknesses, diffusion lengths and recombination velocities of the absorbent layers (CuInSe$_2$ and CuInS$_2$). This study is based on establishing the external quantum efficiency of the two models and the resulting short-circuit photocurrent density by numerical calculation.

This study showed that the model in which the absorber layer with the smallest band gap is placed in the space charge region and the base, gives the greatest efficiency. However, this model may present losses related to the thermalization phenomenon of carriers which are not taken into account in the calculation. The losses related to the interfacial defect are less influenced since the carriers are generated in the space charge region and in a thin part of the base therefore far from the interfaces.

The importance of parameter optimization is more noticeable with the decreasing band gap model where the carriers are first generated in the back areas and follow the path: substrate → base → space charge region. These carriers therefore suffer losses related to the interfacial defects, the influence of the thickness of the base and the diffusion length to reach the space charge region where the collection field reigns. Therefore, the optimization of these parameters is essential to improve the efficiency of this model. This type of structure more exploits the solar spectrum by avoiding the generation of hot carriers which only participate in electrical conduction after thermalization.

The results obtained showed that for standard parameters model (a) gives the best performance. Thus by optimizing the parameters of each model, the study showed on the one hand an evolution of the performances, and on the other hand especially that the two models have practically the same efficiency and give substantially the same performances (external quantum efficiency and short-circuit photocurrent density). Optimizations of manufacturing and sizing parameters are therefore essential for the manufacturer to improve the efficiency of a photovoltaic cell.

Nomenclature

F: Incident photons flux ($cm^{-2}.s^{-1}.eV^{-1}$)
R: Reflection coefficient of region 1 (ZnO)
J_{ph}: Total density of photocurrent ($A.cm^{-2}.eV^{-1}$)
J_{sc}: Short-circuit photocurrent density ($A.cm^{-2}$)
H: Thickness of the structure (μm)
w_1: Thickness of CdS layer in the space charge region (SCR) (μm)
w_2: Thickness of CuInSe$_2$ or CuInS$_2$ layer in the space charge region (SCR) (μm)
w: Thickness of the space charge region (μm)
Absorption coefficient of layer i (cm^{-1}): α_i
Diffusion coefficient in layer i ($cm^2.s^{-1}$): D_{p_i}, D_{n_i}
Diffusion length in layer i (μm): L_{p_i}, L_{n_i}
Recombination velocity (surface or interface) ($cm.s^{-1}$): S_{p_i}, S_{n_i}
Thickness of layer i (μm): H_i
Density (electrons, holes) ($cm^{-3}.eV^{-1}$) in layer i: Δp_i, Δn_i
External quantum efficiency: EQE
J_{w1}: Photocurrent density of holes in CdS layer in the space charge region (SCR) ($A.cm^{-2}.eV^{-1}$)
J_{w2}: Photocurrent density of holes in CuInSe$_2$ or CuInS$_2$ layer in the space charge region (SCR) ($A.cm^{-2}.eV^{-1}$)
q: Elementary charge ($1.6 \times 10^{-19} C$)

Appendix

Table 9. *Discretized values of the energy, the wavelength, the photon fluxes and the external quantum efficiency.*

E (eV)	λ (μm)	Φ(AM0) × 10^{17} (cm^{-2}.s^{-1}. μm^{-1})	Φ(AM1) × 10^{17} (cm^{-2}.s^{-1}. μm^{-1})	Φ(AM1.5) × 10^{17} (cm^{-2}.s^{-1}. μm^{-1})	EQE (a)	EQE (b)
1	1.24	2.834	2.52	2.424	0	0
1.03	1.204	2.96	2.652	2.57	0.026	6.976×10^{-3}
1.06	1.17	3.082	1.523	1.707	0.656	0.125
1.09	1.138	3.201	0.469	0.606	0.748	0.138
1.12	1.107	3.314	2.481	2.247	0.801	0.147
1.15	1.078	3.437	2.975	2.752	0.843	0.154
1.18	1.051	3.57	3.168	2.956	0.867	0.158
1.21	1.025	3.697	3.311	3.106	0.887	0.162
1.24	1	3.817	2.997	2.652	0.905	0.166

E (eV)	λ (µm)	Φ(AM0) × 10^{17} ($cm^{-2}.s^{-1}.\ \mu m^{-1}$)	Φ(AM1) × 10^{17} ($cm^{-2}.s^{-1}.\ \mu m^{-1}$)	Φ(AM1.5) × 10^{17} ($cm^{-2}.s^{-1}.\ \mu m^{-1}$)	EQE (a)	EQE (b)
1.27	0.976	3.932	2.573	2.114	0.923	0.17
1.3	0.954	4.019	1.535	1.212	0.938	0.173
1.33	0.932	4.035	1.035	1.089	0.951	0.176
1.36	0.912	4.05	2.21	1.861	0.962	0.179
1.39	0.892	4.095	2.137	1.764	0.97	0.181
1.42	0.873	4.184	2.121	1.742	0.975	0.183
1.45	0.855	4.281	2.126	1.94	0.979	0.184
1.48	0.838	4.375	3.812	3.71	0.884	0.167
1.51	0.821	4.464	3.827	3.892	0.887	0.17
1.54	0.805	4.548	4.17	3.749	0.888	0.175
1.57	0.79	4.594	4.226	4.038	0.889	0.19
1.6	0.775	4.638	4.279	4.011	0.89	0.274
1.63	0.761	4.68	3.297	3.212	0.891	0.407
1.66	0.747	4.721	4.292	4.091	0.891	0.562
1.69	0.734	4.76	4.126	3.933	0.892	0.651
1.72	0.721	4.798	4.325	4.105	0.892	0.716
1.75	0.709	4.835	4.348	4.101	0.893	0.753
1.78	0.697	4.865	4.349	4.098	0.893	0.785
1.81	0.685	4.891	4.338	4.094	0.893	0.801
1.84	0.674	4.916	4.328	4.091	0.893	0.814
1.87	0.663	4.94	4.318	4.046	0.893	0.825
1.9	0.653	4.963	4.287	4.001	0.893	0.834
1.93	0.642	4.986	4.256	3.957	0.893	0.842
1.96	0.633	5.008	4.227	3.914	0.892	0.849
1.99	0.623	5.029	4.199	3.873	0.892	0.856
2.02	0.614	5.049	4.171	3.833	0.892	0.861
2.05	0.605	5.069	4.167	3.812	0.892	0.866
2.08	0.596	5.076	4.167	3.796	0.891	0.87
2.11	0.588	5.022	4.12	3.738	0.891	0.873
2.14	0.579	4.915	4.029	3.641	0.891	0.876
2.17	0.571	4.811	3.939	3.545	0.89	0.879
2.2	0.564	4.811	3.882	3.485	0.89	0.881
2.23	0.556	4.811	3.866	3.485	0.89	0.883
2.26	0.549	4.84	3.868	3.485	0.889	0.884
2.29	0.541	4.931	3.871	3.485	0.889	0.885
2.32	0.534	4.939	3.871	3.448	0.889	0.885
2.35	0.528	4.858	3.773	3.333	0.888	0.886
2.38	0.521	4.773	3.773	3.333	0.888	0.886
2.41	0.515	4.885	3.784	3.333	0.887	0.886
2.44	0.508	4.909	3.788	3.333	0.884	0.884
2.47	0.502	4.909	3.787	3.333	0.877	0.877
2.5	0.496	4.858	3.696	3.244	0.854	0.854
2.53	0.49	4.976	3.762	3.22	0.795	0.795
2.56	0.484	4.991	3.761	3.214	0.653	0.653
2.59	0.479	4.845	3.682	3.11	0.507	0.507
2.62	0.473	4.825	3.606	3.012	0.496	0.496
2.65	0.468	4.805	3.531	2.933	0.484	0.484
2.68	0.463	4.786	3.458	2.855	0.473	0.473
2.71	0.458	4.675	3.353	2.737	0.462	0.462
2.74	0.453	4.374	3.179	2.532	0.451	0.451
2.77	0.448	4.079	3.01	2.332	0.44	0.44
2.8	0.443	3.791	2.843	2.136	0.43	0.43
2.83	0.438	3.545	2.681	1.965	0.419	0.419
2.86	0.434	3.596	2.522	1.931	0.409	0.409
2.89	0.429	3.701	2.366	1.898	0.399	0.399
2.92	0.425	3.712	2.348	1.865	0.389	0.389
2.95	0.42	3.712	2.348	1.833	0.379	0.379
2.98	0.416	3.544	2.231	1.65	0.37	0.37
3.01	0.412	3.236	2.016	1.342	0.202	0.202
3.04	0.408	2.935	1.804	1.058	0.183	0.183
3.07	0.404	2.639	1.597	1.018	0.164	0.164
3.1	0.4	2.348	1.394	0.98	0.146	0.146
3.13	0.396	2.197	1.271	0.942	0.128	0.128
3.16	0.392	2.197	1.236	0.905	0.109	0.109
3.19	0.389	2.197	1.202	0.868	0.091	0.091
3.22	0.385	2.197	1.168	0.832	0.075	0.075
3.25	0.382	2.197	1.135	0.797	0.062	0.062

E (eV)	λ (µm)	Φ(AM0) × 10^{17} ($cm^{-2}.s^{-1}.\ \mu m^{-1}$)	Φ(AM1) × 10^{17} ($cm^{-2}.s^{-1}.\ \mu m^{-1}$)	Φ(AM1.5) × 10^{17} ($cm^{-2}.s^{-1}.\ \mu m^{-1}$)	EQE (a)	EQE (b)
3.28	0.378	2.197	1.103	0.763	0.051	0.051
3.31	0.375	2.132	1.066	0.729	0.042	0.042
3.34	0.371	2.057	1.028	0.695	0.034	0.034
3.37	0.368	1.983	0.992	0.663	0.028	0.028
3.4	0.365	1.95	0.955	0.63	0.026	0.026
3.43	0.362	1.926	0.92	0.599	0.026	0.026
3.46	0.358	1.903	0.885	0.568	0.027	0.027
3.49	0.355	1.88	0.851	0.537	0.028	0.028
3.52	0.352	1.858	0.817	0.507	0.029	0.029
3.55	0.349	1.836	0.784	0.478	0.029	0.029
3.58	0.346	1.814	0.749	0.446	0.03	0.03
3.61	0.343	1.793	0.704	0.403	0.03	0.03
3.64	0.341	1.772	0.659	0.361	0.03	0.03
3.67	0.338	1.751	0.616	0.32	0.03	0.03
3.7	0.335	1.695	0.573	0.279	0.03	0.03
3.73	0.332	1.615	0.53	0.239	0.03	0.03
3.76	0.33	1.536	0.489	0.2	0.03	0.03
3.79	0.327	1.459	0.416	0.161	0.03	0.03
3.82	0.325	1.397	0.318	0.123	0.029	0.029
3.85	0.322	1.34	0.221	0.085	0.029	0.029
3.88	0.32	1.285	0.125	0.048	0.029	0.029

References

[1] M. Powalla, E. Lotter, R. Waechter, S. Spiering, M. Oertel, B. Dimmler, "Pilot line production of CIGS modules: first experience in processing and further developments", Proc. 29th IEEE Photovoltaic Specialists Conf., New Orleans, 2002, p. 5 71.

[2] J. Kessler, M. Bodegard, J. Hedstrom and L. Stolt, "New world record Cu(In,Ga)Se, based mini-module: 16.6%", Proc. 16 th European Photovoltaic Solar Energy Conf., Glasgow, 2000, p. 2057.

[3] M. Contreras, B. Egaas, K. Ramanathan, J. Hiltner, A. Swartzlander, F. Hasoon and R. Noufi, "Progress toward 20% efficiency in Cu(In,Ga)Se_2 polycrystalline thin-film solar cells", Prog. Photovolt. Res. Appl. Vol. 7, 1999, p. 311.

[4] J. F. Guillemoles, P. Cowache, A. Lusson, K. Fezzaa, F. Boisivon, J. Vedel and D. Lincot, "High quality $CuInSe_2$ epitaxial films-molecular beam epitaxial growth and intrinsic properties", J, Appl. Phys., Vol. 79, 1996, p. 7293.

[5] C. Eberspacher, K. L. Pauls and C. V. Fredric, "Improved processes for forming $CuInSe_2$ films", Proc. 2nd World Conf. on Photovoltaic Solar Energy Conversion, Vienna, 1998, p. 303.

[6] K. Ramanathan, R. N. Bhattacharya, J. Granata, J. Webb, D. Niles, M. A. Contreras, H. Wiesner, F. S. Haason and R. Noufi, "Advances in the CIS research at NREL", Proc. 26th IEEE Photovoltaic Specialists Conf., Anaheim, 1998, p. 319.

[7] D. Lincot, J.-F. Guillemoles, P. Cowache, A. Marlot, C. Lepiller, B. Canava, F. B. Yousfi and J. Vedel, "Solution deposition technologies for thin film solar cells: status and perspectives", Proc. 2nd World Conf. on Photovoltaic Solar Energy Conversion, Vienna, 1998, p. 440.

[8] F. Karg, D. Kohake, T. Nierhoff, B. Kuhne, S. Grosser and M. C. Lux-Steiner, "Performance of grid-coupled PV arrays based on CIS solar modules", Proc. 17th European Photovoltaic Solar Energy Conf., Munich, 2002, p. 391.

[9] R. R. Gay, "Status and prospects for CIS-based photovoltaics", Solar Energy Mater. Solar Cells, Vol. 47, 1997, p. 19.

[10] E. M. Keita, B. Ndiaye, M. Dia, Y. Tabar, C. Sene, B. Mbow,"Theoretical Study of Spectral Responses of Heterojunctions Based on $CuInSe_2$ and $CuInS_2$" OAJ Materials and Devices, Vol 5#1, 0508 (2020) – DOI: 10.23647/ca.md20200508.

[11] Subba Ramaiah Kodigala, "Cu($In_{1-x}Ga_x$)se_2 based thin solar cells", 2010, Volume 35, Academic Press, ELSEVIER. Inc.

[12] T. Loher, W. Jaegermann, C. Pettenkofer, "Formation and electronic properties of the CdS/$CuInSe_2$ (011) heterointerface studied by synchrotron-induced photoemission", J. Appl. Phys. 77 (1995) 731.

[13] H. Hahn, G. Frank, W. Klinger, A. D. Meyer, G. Stroger, "Über einige ternäre Chalkogenide mit Chalcopyritestruktur", Z. Anorg. Aug. Chem. 271 (1953) 153.

[14] Liann-Be Chang, Chzu-Chiang Tseng, Gwomei Wu, Wu-Shiung Feng, Ming-Jer Jeng, Lung-Chien Chen, Kuan-Lin Lee, Ewa Popko, Lucjan Jacak and Katarzyna Gwozdz, ''Low-Cost $CuIn_{1-x}Ga_xSe_2$ Ultra-Thin Hole-Transporting Material Layer for Perovskite/CIGSe Heterojunction Solar Cells'', Appl. Sci. 2019, 9, 719; doi:10.3390/app9040719.

[15] Anjun Han, Yi Zhang, Wei Song, Boyan Li, Wei Liu and Yun Sun," Structure, morphology and properties of thinned Cu(In, Ga)Se_2 films and solar cells'', Semicond. Sci. Technol. 2012, 27, 3.

[16] S. J. Fonash, Solar Cell device Physics, Academic Press, New York, 1981.

[17] H. L. Hwang, C. Y. Sun, C. Y. Leu, C. C. Cheng, C. C. Tu, "Growth of $CuInS_2$ and its characterization", Rev. Phys. Appl. 13 (1978) 745.

[18] E. M. Keita, B. Mbow, M. S. Mane, M. L. Sow, C. Sow, C. Sene "Theoretical Study of Spectral Responses of Homojonctions Based on $CuInSe_2$" Journal of Materials Science & Surface Engineering, Vol. 4 (4), 2016, pp392-399.

[19] S. B. Zhang, Su-Huai Wei, and Alex Zunger, “Stabilization of Ternary Compounds via Ordered Arrays of Defect Pairs”, Phys. Rev. Lett, 1997, vol. 78, 4059.

[20] Abazović Nadica D., Jovanović Dragana J., Stoiljković Milovan M., Mitrić Miodrag N., Ahrenkil Phillip S., Nedeljković Jovan M., Čomor Mirjana I., “Colloidal-chemistry based synthesis of quantized $CuInS_2/Se_2$ nanoparticles”, Journal of the Serbian Chemical Society, 2012, Volume 77, Pages: 789-797.

[21] R. Noufi, R. Axton, C. Herrington and S. K. Deb, “Electronic properties versus composition of thin films of $CuInSe_2$”, Appl. Phys. Lett., Vol. 45, 1984, p. 668.

[22] P. Migliorato, J. L. Shay, H. M. Kasper and S. Wagner, “Analysis of the electrical and luminescent properties of $CuInSe_2$”, J. AppI. Phys. Vol. 46, 1975, p. 1777.

[23] E. M. Keita, Y. Tabar, B. Ndiaye, A. A. Correa, C. Sene, B. Mbow, “Modeling and Analysis of the Effects of Surface and Interface States on the Photocurrent and the Efficiency of a Solar Cell Based on n^+npp^+ Structure”, Int. J. Adv. Sci. Eng. Vol. 8 No. 3, 2022, p. 2328-2340. https://doi.org/10.29294/IJASE.8.3.2022.2328-2340

[24] Hisashi Yoshikawa, Sadao Adachi. 1997. Optical Constants of ZnO, Jpn. J. Appl. Phys. 36, 6237-6243.

[25] B. MBOW, A. MEZERREG, N. REZZOUG, and C. LLINARES, “Calculated and Measured Spectral Responses in Near-Infrared of III-V Photodetectors Based on Ga, In, and Sb”, phys. Stat. Sol. (a) 141, 511 (1994).

[26] H. J. HOVEL and J. M. WOODALL, “$Ga_{1-x}Al_xAs$ - GaAs P-P-N Heterojunction Solar Cells”, J. Electrochem. Soc. 120, 1246 (1973).

[27] H. J. HOVEL and J. M. WOODALL, 10th IEEE Photovoltaic Specialists Conf., Palo Alto (Calif.) 1973 (p. 25).

[28] El Hadji Mamadou KEITA, 2017. Doctoral Thesis, Etude théorique de réponses spectrales de cellules solaires à base de $CuInSe_2$: Modèles à 2 couches (p/n et n/p), à 3 couches (p/n/n+, p+/p/n, n/p/p+ et n+/n/p) et à 4 couches (p+/p/n/n+ et n+/n/p/p+), Université Cheikh Anta DIOP de Dakar, Sénégal P. 24-47.

[29] E. M. Keita, B. Mbow, C. Sene, ‘' Perovskites and other framework structure crystalline materials”, chap No 22: Framework structure materials in photovoltaics based on perovskites 3D”, OAJ Materials and Devices, vol 5 (2), (Coll. Acad. 2021), p. 637-708. DOI: 10.23647/ca.md20201511.

[30] Alain Ricaud, “Photopiles Solaires”, de la physique de la conversion photovoltaïque aux filières, matériaux et procédés. 1997, 1e édition, Presses polytechniques et universitaires romandes, p. 40.